VIII International Conference on Fracture Mechanics of Concrete and Concrete Structures
FraMCoS-8
J.G.M. Van Mier, G. Ruiz, C. Andrade, R.C. Yu and X.X. Zhang (Eds)

A NEW MODEL TO FORECAST THE RESPONSE OF CONCRETE STRUCTURES UNDER SEVERE LOADINGS: THE μ DAMAGE MODEL

J. MAZARS [*], F. HAMON[†]

[*] Grenoble Institute of Technology (lab. 3SR), BP 53, 38041 Grenoble (France)
e-mail: jacky.mazars@grenoble-inp.fr

[†] EDF – DER
e-mail: francois.hamon@edf.fr

Key words: Damage models, Unilateral behavior, Cyclic loading, Concrete, Severe loading, Finite element calculations.

Abstract: The estimate of the ultimate capacity of a concrete structure is essential to determine the safety margins. The evolutions of regulations and the desire to build sustainable structures lead engineering to dispose modelling tools simple and efficient. In this spirit we present here a 3D unilateral model (μ model) based on the coupling of elasticity and damage in an isotropic formulation. Based on the damage model from Mazars, the introduction of unilateral behaviour comes from the use of two internal variables. A threshold surface is associated to each of these variables. Their shape was chosen to model the best behaviour of concrete under various loading: tension, compression, shear, biaxial and triaxial loadings. Applications are presented at the material level (Gauss point) and on a reinforced concrete structure. Comparison with experimental results shows the effectiveness of selected options.

1 INTRODUCTION

Concrete, like the majority of geomaterials and ceramics, is perceived as brittle in tension and more ductile under a compressive loading. During loading, a network of microscopic cracks nucleates perpendicularly to the direction of extension, with these cracks coalescing until the point of complete rupture. Whereas under uniaxial tension just a single crack propagates, under compression and in the presence of heterogeneities (aggregate surrounded by a cement matrix), transverse tensile strains generate a self-equilibrated stress field orthogonal to the loading direction. A pure mode I (extension) is thus considered for the purpose of describing the behaviour in both tension and compression. When the material is confined, mode II is favoured and, afterwards, a threshold hydrostatic pressure serves to compact the porous cement matrix.

Within this framework, it has been shown (Mazars [1]) that essentially three distinct damage modes need to be considered:

A) a situation dominated by mode I relative to local extension ($\varepsilon_i > 0$);

B) a situation dominated by mode II without any local extension;

C) a situation relative to the application of strong hydrostatic pressure, leading to compaction (pore collapse in the cement matrix).

To simulate the behaviour of concrete, either plasticity (Ottosen [2]), damage models (Mazars [1], Mazars *et al.* [3], Jirasek [4], Desmorat *et al.* [5]) or fracture-based approaches (Bazant [6]) are used. These approaches are adapted so as to simulate situation "A" above, which is the one most often found in conventional reinforced concrete structures.

Number of models allow for describing the cyclic behaviour [7, 8], including that generated by earthquakes, and some are capable of simulating severe loadings such as those caused by blast or impacts (situations B and C seen above - [9, 10]).

An early model set up for concrete in such a context, but limited to monotonous loadings, is the damage Mazars model [1]. On this basis, we propose a new model (the μ model) with emphasis on simplicity and the ability to describe the main aspects of the conduct described above, including unilaterality (opening and closing of cracks). A series of numerical applications are presented including a comparison with experimental results demonstrates the effectiveness of modelling.

2 MODELLING CONCEPTS: μ MODEL

Developed in the framework of thermodynamics of irreversible processes, the μ model, the principles of which are presented below, is based on the Mazars model [1]. In the framework of an elasticity-damage coupling, the behaviour is given by:

$$\underline{\underline{\sigma}} = (1 - D_\mu)\underline{\underline{\underline{\underline{E}}}} : \underline{\underline{\varepsilon}} \qquad (1)$$

$\underline{\underline{\underline{\underline{E}}}}$ is the stiffness matrix of undamaged material, $\underline{\underline{\sigma}}$ and $\underline{\underline{\varepsilon}}$ are the stress and strain tensors respectively. D_μ is the damage variable, a scalar (damage is assumed isotropic) which evolves from 0 (undamaged material) to 1 (failure).

2.1 Unilateral description

To describe the unilateral nature of concrete, we opted for the use of two internal variables. However, unlike the classical models [7], [9]), they are not the damage variables. In the μ model the internal variables are defined from two equivalent deformations $\varepsilon_{\mu t}$ and $\varepsilon_{\mu c}$ (scalar indicators of the state of local strain). $\varepsilon_{\mu t}$ favours tensile strain and $\varepsilon_{\mu c}$ favours compression strains. Their expressions were chosen to improve the modelling of concrete behaviour in shear and bi-compression over the original model which underestimates these properties.

$$\varepsilon_{\mu t} = \frac{I_\varepsilon}{2(1-2\upsilon)} + \frac{\sqrt{J_\varepsilon}}{2(1+\upsilon)} \qquad (2)$$

$$\varepsilon_{\mu c} = \frac{I_\varepsilon}{5(1-2\upsilon)} + \frac{6\sqrt{J_\varepsilon}}{5(1+\upsilon)} \qquad (3)$$

ν is the Poisson's ratio, I_ε is the first invariant of the strain tensor and J_ε , the second invariant of the deviatoric of the strain tensor:

$$I_\varepsilon = \varepsilon_1 + \varepsilon_2 + \varepsilon_3 \qquad (4)$$

$$J_\varepsilon = \frac{1}{2}[(\varepsilon_1 - \varepsilon_2)^2 + (\varepsilon_2 - \varepsilon_3)^2 + (\varepsilon_3 - \varepsilon_1)^2] \qquad (5)$$

ε_i are the principal strains.

From this, the expressions for the two internal variables, $Y_{\mu t}$ and $Y_{\mu c}$ are:

$$Y_{\mu t} = \max(\varepsilon_{\mu t0}, \max(\varepsilon_{\mu t})) \qquad (6)$$

$$Y_{\mu c} = \max(\varepsilon_{\mu c0}, \max(\varepsilon_{\mu c})) \qquad (7)$$

They are the maximum equivalent strain reached, beyond a threshold ($\varepsilon_{\mu t0}$ and $\varepsilon_{\mu c0}$), during the loading history. They are each associated with a loading surface. As Drucker Prager model [11], the two loading surfaces are cones centered on the trisectrice of the strain space. They operate independently of each other.

$$f_{\mu t} = \varepsilon_{\mu t} - Y_{\mu t} = 0 \qquad (8)$$

$$f_{\mu c} = \varepsilon_{\mu c} - Y_{\mu c} = 0 \qquad (9)$$

The second new feature, compared to the original model, is managing the damage variable, denoted D_μ. This variable is controlled by the variable Y_μ, a combination of both internal variables $Y_{\mu t}$ and $Y_{\mu c}$:

$$Y_\mu = rY_{\mu t} + (1-r)Y_{\mu c} \qquad (10)$$

r is the triaxiality factor, which provides information on the actual loading state [12]. It is equal to 1 in the traction area and to 0 in the compression area. It takes intermediate values for tension-compression situations. Its expression is:

$$r = \frac{\sum_i \langle \tilde{\sigma}_i \rangle_+}{\sum_i |\tilde{\sigma}_i|} \qquad (11)$$

|x| and $\langle x \rangle_+$ are the absolute and the positive values of x respectively. $\tilde{\sigma}_i$ is the effective stress [13] which is easy to calculate :

$$\tilde{\sigma}_i = \frac{\sigma_i}{(1 - D_\mu)} \qquad (12)$$

The damage evolution law is the same type as the original model. Its expression is:

$$D_\mu = 1 - \frac{(1-A)Y_{\mu 0}}{Y_\mu} - A \exp\left(-B\left(Y_\mu - Y_{\mu 0}\right)\right) \qquad (13)$$

$Y_{\mu 0}$ is the initial threshold of the pilot variable Y_μ, function of the equivalent strain thresholds defined equations (2) and (3):

$$Y_{\mu 0} = r\varepsilon_{\mu t 0} + (1-r)\varepsilon_{\mu c 0} \qquad (14)$$

A and *B* are two variables which depends on the actual loading state through the r value. They allow to reproduce the different behaviours from quasi brittle to hardening including mixed situation due to shear effects. The following evolution for *A* and *B* has been chosen:

$$A = A_t\left(2r^2(1-2k) - r(1-4k)\right) + A_c\left(2r^2 - 3r + 1\right) \qquad (15)$$

$$B = r^2 B_t + (1 - r^2) B_c \qquad (16)$$

A_t, B_t, A_c and B_c are all material parameters, just like in the original model and k the ratio A/At used to calibrate pure shear behaviour.

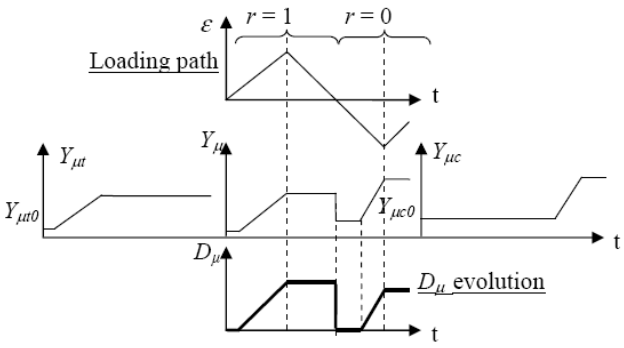

Figure 1 : Evolution of internal variables $Y_{\mu t}$ and $Y_{\mu c}$, their combination Y_μ. And damage D_μ, during a tension – compression loading.

(13) induces, and this is the new compared to other unilateral models, an irregular evolution of the damage variable since it depends on r. However the variables $Y_{\mu t}$ and $Y_{\mu c}$ are continuously increasing, it is the reason why they are chosen as internal variables (see Figure 1 the various evolutions during a tension-compression loading).

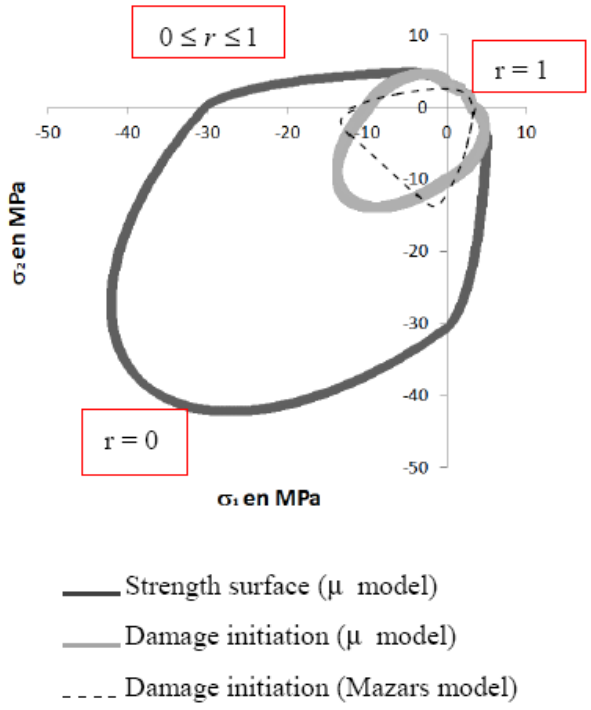

Figure 2: In the plane σ_3=0, surface of failure and damage initiation surface (for μ and Mazars models). Numerical values are for an ordinary concrete (fc=30MPa)

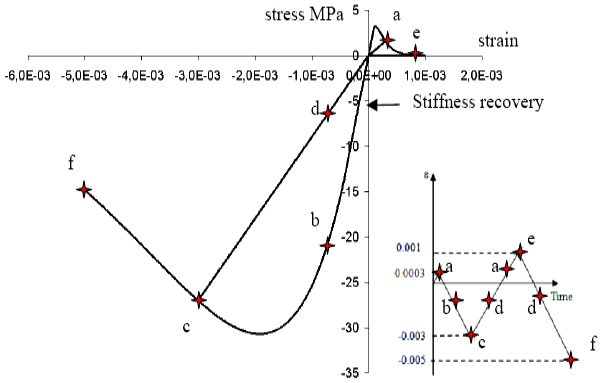

Figure 3: Tension-compression loading path exhibiting unilateral effect.

Figure 2 shows, in the plane $\sigma_3 = 0$, the trace of the surface initiation of damage ($D_\mu = 0$) and this of failure (maximum stress envelop). The surface initiation of the original

model is also presented, for comparison. Fig. 3 shows the unilateral response of the μ model for a tension-compression loading path.

2.2 Severe loadings

This section presents the procedure for simulating the effects of confinement using the same model. Confinement corresponds to loadings in the tri-compression domain. The triaxiality factor *r* introduced equation (11) is, within the confinement domain, equal to 0. As presented section 1, various damage modes exists depending on the presence or not of extensions. At this point, two separate domains can be considered:

- Extension Allowed zone ("EA" zone), when during loading a positive strain on at least one direction exists;
- No Extension Allowed zone ("NEA" zone), when loading forbids any kind of extension.

The following subsection will be divided into two parts: the "EA" zone and "NEA" zone.

1) Extension Allowed Zone ("EA" zone)

The loading state in this zone is: $\sum<\varepsilon_i>_+ \neq 0$, which can be written as $I_{\varepsilon+} \neq 0$. This zone is the domain of "low confinement". A confinement coefficient *C* is introduced in order to model confinement effects within the EA zone. This coefficient affects the internal variable $Y_{\mu c}$. When $r = 0$, the variable Y_μ (41) that controls damage then becomes:

$$Y_\mu = C\, Y_{\mu c} \qquad (17)$$

C is an indicator of the existence of local extension and has been defined as follows:

$$\begin{cases} C = 1 & \text{if } r > 0 \\ C = \dfrac{\sum \langle \varepsilon_i \rangle_+}{\sum \langle \varepsilon_{i0} \rangle_+} \Leftrightarrow C = \dfrac{I_{\varepsilon+}}{I_{\varepsilon 0+}} & \text{if } r = 0 \end{cases} \qquad (18)$$

$I_{\varepsilon 0+}$ is the projection of $I_{\varepsilon+}$ on the nearest plane σ_i=0. $I_{\varepsilon 0+}$ is thus calculated by setting at 0 the "strongest" stress (i.e. the lowest in absolute value terms) of the three principal stresses. From these equations, D_μ can be calculated according to a classical approach using (13).

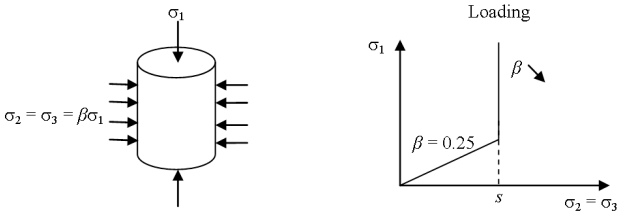

Figure 4: Sample and loading path

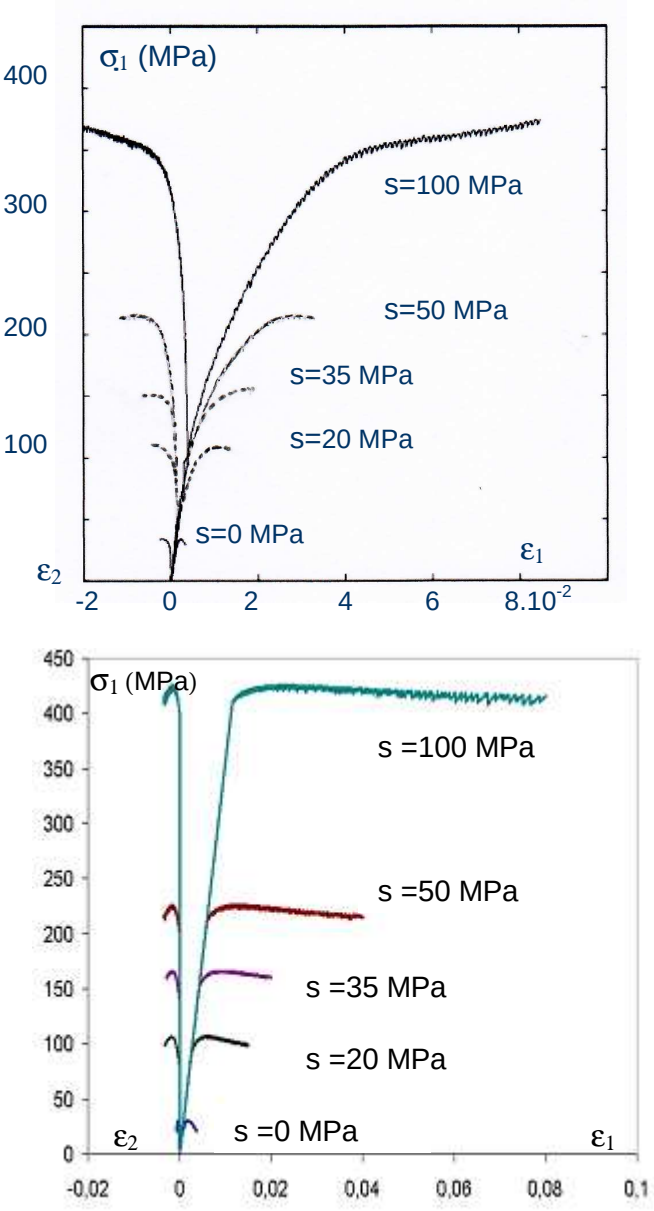

Figure 5: Triaxial test, after a radial path $\sigma_2 = \sigma_3 = s$ and with σ_1 increasing until failure - Top: experimental results (Ramtani [14], Gabet [15]) - Down: μ model simulations.

To analyze the model response within the EA zone, a cylindrical sample subjected to a vertical compression σ_1 and a confinement $\sigma_2=\sigma_3$ is considered (see Figure 4). This test can be conducted in a cell adapted for concrete specimens.

The loading path comprises 2 steps:

a/ radial path: $\sigma_2 = \sigma_3 = \beta\sigma_1$ (where β is a constant)

b/ triaxial path: $\sigma_2 = \sigma_3 =$ s (s is fixed) and σ_1 increases until failure.

When ν equals 0.2, it is straightforward to show that $C = 0$ for β greater than or equal to 0.25. To avoid any damage during the first step, β = 0.25 has been chosen. Afterwards, during the second step, β (= s/σ_1) decreases, so that D_μ can evolve until failure.

The down side of Figure 5 displays the results given for the same concrete used earlier, for *s* values of 0, 20, 35, 50 and 100 MPa. The top side of Figure 5 presents the experimental results obtained by two researchers on a similar concrete (Ramtani [14], Gabet [15]). It can be observed that the trends and values at failure have been correctly simulated (except for *s* = 100 MPa, the relevant explanation will be provided below).

2) No Extension Allowed Zone ("NEA" zone)

The loading state in this zone is $I_{\varepsilon+}= 0$; it corresponds to the "high confinement" domain. As revealed in Table 1, two distinct damage modes can be activated:

- Due to high hydrostatic pressure, after a threshold (I_σ - $I_{\sigma 0}$ = 0), the microporous matrix gradually compacts, which in turn induces damage $D_{\mu hc}$ in addition to $D_{\mu c}$ that evolves until the compaction process is complete and then acts upon the bulk modulus.

- Due to the application of a deviator, a material "flow" leads to failure after a strong distortion ($\gamma_{12} = 2\varepsilon_{12} > 10^{-2}$). This type of behaviour has been observed following a threshold in the ($\sqrt{J_\sigma}$, I_σ) plane during specific experiments performed on the GIGA machine at the 3S-R Laboratory in Grenoble (Gabet [15]). This phenomenon may be described by introducing a new damage variable D_{sh} coupled with D_μ.

At a high *s* value (i.e. 100 MPa in figure 5), it would appear that both phenomena described for the NEA zone have been activated. In this case, $D_{\mu hc}$ and D_{sh} will increase, meaning that the failure simulated Figure 5 (σ_{1max} # 420MPa), by only taking into account low confinement effects (i.e. the EA zone), cannot be correct. Real failure would be lower, as indicated on the experimental results (top side of figure 5, σ_{1max} # 370MPa).

This part of the model is still being developed as are other options such as hysteretic effects and strain rate effects, which are easy to introduce through an evolution of the initial thresholds ($Y_{\mu t0}$, $Y_{\mu c0}$) with respect to the local strain velocity, as introduced in the PRM model (Pontiroli *et al.* [9]). Severe loadings will thus not be considered in the next section.

3 NUMERICAL SIMULATIONS

3.1 Implementations

Even though the μ model can be applied to simulate complex cases, its equations and implementation remain quite simple. As with the original model, its formulation is explicit, meaning that all variables can be evaluated directly from the strain increment. With the strain increment, $\Delta\underline{\underline{\varepsilon}}$, provided by the finite element code, the principal strains, ε_i, and principal effective stresses, $\tilde{\sigma}_i$ (12), are calculated. *r* can thus be obtained using (11). With this variable and material parameters A_t, A_c, B_t, B_c and k it is possible to evaluate variables *A*, (15), and *B*, (16). Next, the equivalent strains, $\varepsilon_{\mu t}$ and $\varepsilon_{\mu c}$, are calculated from the principal strains. The internal variables $Y_{\mu t}$ and $Y_{\mu c}$ are given in (6) and (7), respectively. If $\varepsilon_{\mu t}$ (or $\varepsilon_{\mu c}$) is greater than the previous values of $Y_{\mu t}$ (or $Y_{\mu c}$, respectively) from the *n*-1 increment, then the corresponding internal variable is equal to the

highest value of $\varepsilon_{\mu t}$ (or $\varepsilon_{\mu c}$) at increment *n*. $Y_{\mu t}$ is calculated independently of $Y_{\mu c}$. Consequently, (8) and (9) are verified at each increment. The next step consists of combining $Y_{\mu t}$, $Y_{\mu c}$ and r in order to obtain Y_μ and D_μ, (10) and (13), respectively. And lastly, the stresses are given by (1).

It can be observed that the entire model is described using 8 parameters, including Young's modulus and Poisson's ratio, all, identified from just two series of tests (uniaxial tension and uniaxial compression), which makes this model relevant for engineering applications.

3.2 Validation Tests

Kupfer *et al.* [16] completed a series of tests to investigate the response of plain concrete subjected to two-dimensional loading. During these investigations, concrete plates (200 mm by 200 mm by 50 mm) were loaded until failure at prescribed ratios of σ_1/σ_2, with σ_3 equal to zero. σ_i denotes the principal stresses.

The concrete characteristics are listed table 1. Model parameters have been fitted to obtain the same strengths (f_t, f_c) under uniaxial tensile and uniaxial compressive loadings.

Table 1: *Experimental data*

E_0 (MPa)	34000
ν	0.19
f_t (MPa)	3.27
f_c (MPa)	-32.7

The results from running the μ models and the original Mazars model have been compared for a bi-compression with the ratio $\omega=\sigma_1/\sigma_2$ = 0.52. In is important to note that for both model only the characteristics in Table 1 have been fixed, it is then a real prediction. At the top of the curve, due to loading controls, the final experimental point corresponds to the collapse of the specimen.
The original model underestimates the strength, and the structure collapses too quickly for this loading case, while the μ model give a very good prediction of the maximum strength and quite good results for the strain evolutions on both direction.

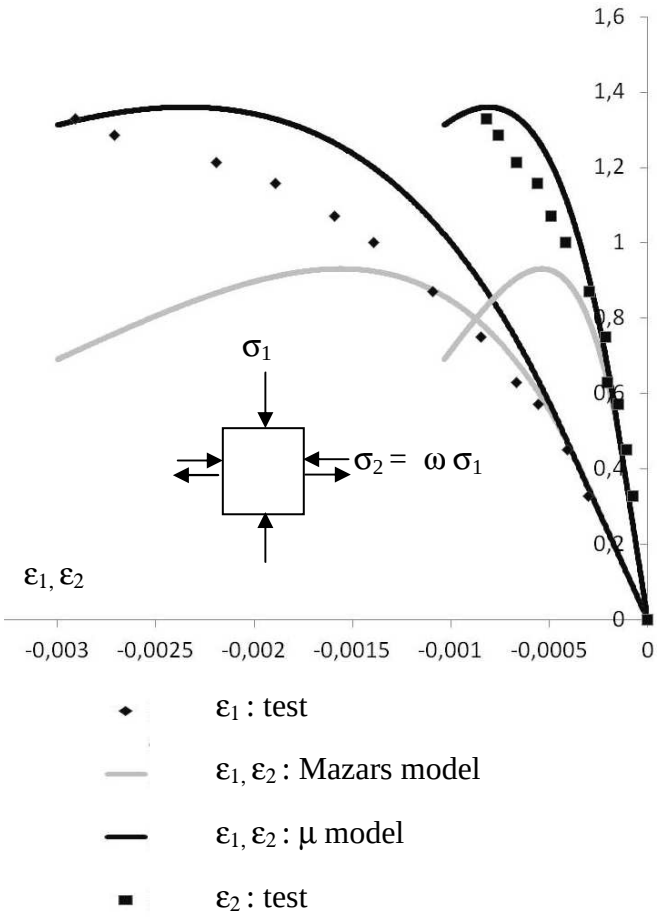

Figure 6: Comparison between numerical curves and experimental points from Kupfer *et al.* [16] for a biaxial compression loading ω = 0.52

3.3 Cyclic bending test on a reinforced concrete beam

Another major difference between the original and the μ model is highlighted by cyclic loadings, since it takes into account the stiffness recovery due to crack closure. The three-point bending test performed by La Borderie [17] has thus been simulated in order to compare model responses. The specimen is a concrete beam reinforced by four 12mm diameter rebar elements. The geometry and all dimensions of the structure are illustrated in Figure 7. The test specimen has been modelled using *Code_Aster*® QU4 (four-node) elements under a plane strain assumption. Boundary conditions are defined to correctly represent the experimental test (Figure 7); these conditions change with the sign of the

displacement. U_y, applied at the middle of the beam, follows a cyclic evolution.

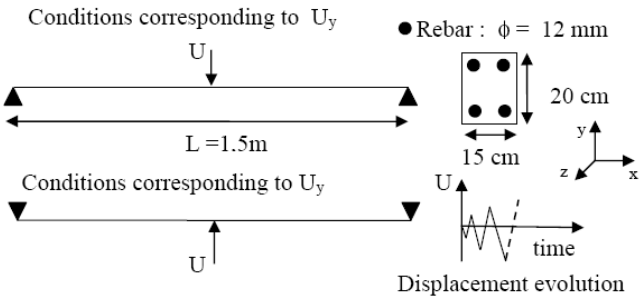

Figure 7: Bending test, size, boundary conditions and loading path [17]

Table 2: Displacement values during the test [17]

Increment	Displacement U_y (m)
0	0
1	-0.001
2	0
3	0.001
4	0
5	-0.0015

Depending on the supports used during the experiments, these supports can be modelled by an elastic part (same stiffness as the concrete), while displacements are applied on the rigid supports (Fig. 8a). In order to avoid mesh sensitivity, crack band approach utilizing fracture energy has been used in this application (Bazant et al. [18]).

The selected model parameter values have been adopted in accordance with the data provided by La Borderie [17].

In Figure 8b,c, the load-displacement curves resulting from the simulations are compared to the experimental points. Over the first part of the loading (increment 1 table 2, negative displacements), the two model responses are all similar.

When the displacement is positive (increment 3 table 2), the numerical curves differ considerably. With the μ model, stiffness is recovered while such is not the case with the original model. As opposed to the μ model, the damage variable D of the original model is the same as for increment 1, then, when the displacement sign changes, the concrete remains "damaged".

For the third part of the loading (Fig. 8c), the μ model curve follows the sequence of experimental points; it reaches the same load value by the end of the test.

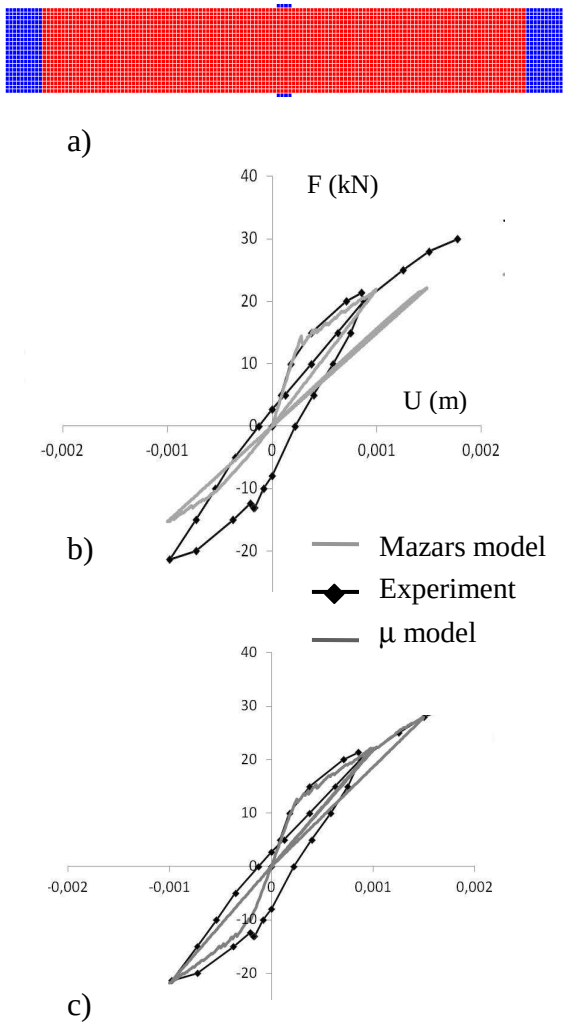

Figure 8: Bending test- a) Finite element mesh – b) Comparison experiment – calculation with the Mazars model – c) Comparison experiment-calculation for the μ model showing the unilateral response.

Figure 9 shows that during a cyclic loading, damage evolves until reaching a maximum value in one direction; due to changes in the triaxial factor r from 1 to 0, this maximum value vanishes when the local stress is reversed. This property can be used as a crack opening indicator. Figure 9 also provides the situation with D_μ (the red marks indicate where $0.95 < D_\mu < 1$, which corresponds to a

crack opening stage) for three different steps: increments 1, 2 and 3, respectively (see table 2). From top to bottom, the following can be observed: 1) Fig. 9a, the cracks open during the initial loading on the lower part of the beam; 2) Fig. 9b, at zero loading, the main previous cracks are closed; and 3) Fig. 9c, cracks open during the second loading, on the upper part of the beam, with some of these joining cracks already open during the first stage of loading that subsequently reopen.

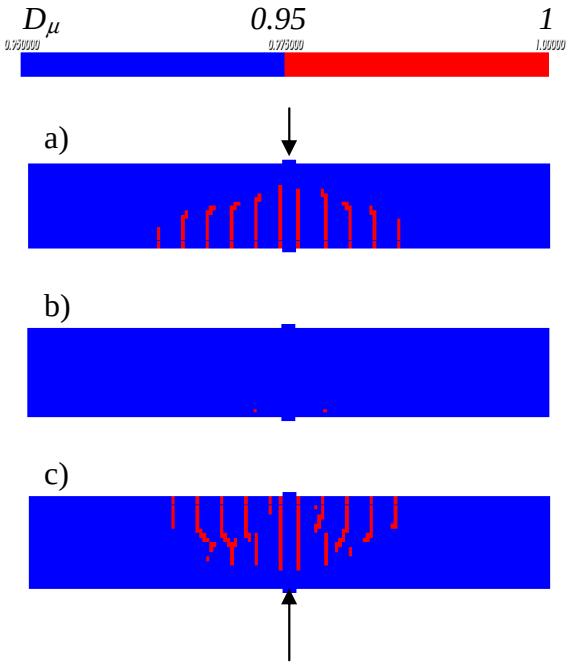

Figure 9: Visualization of the damage variable D_μ during the 3-point bending test (red corresponds to $0.975 < D_\mu < 1$) - a) First part of the loading U_y = -0.001 m - b) The displacement has increased to 0 m c) Second part of the loading U_y = 0.001 m

These results reveal the efficiency of the μ model, which has proven to be robust and efficient in describing both cyclic behaviour and crack opening behaviour.

4 CONCLUSIONS

Built on similar principles as the original Mazars model, and by including two internal variables, the "μ model" takes into account, within a 3D formulation, the unilateral behaviour of concrete (crack opening and closure), which is essential for cyclic loadings, particularly for the seismic behaviour of concrete structures. In the tri-compression domains, two cases have been considered. The first is the "low confinement" domain, i.e. when the load allows for extensions ($\sum\langle\varepsilon_i\rangle_+ \neq 0$), whose behaviour has also been discussed. The second case is the "high confinement" domain, which is still under development. Other advances are also underway, including, as for the original model, a non local description [19, 20], the introduction of rate effects and hysteretic behaviour to accommodate dynamic loadings at low or high speeds, such as impacts capable of inducing penetration and perforation [9].
Built around a simple formulation that combines elasticity and damage and by respecting the thermodynamic principles of irreversible processes, this model is easy to implement in a finite element code. Furthermore, the material parameters (total 8, including elastic parameters) are easily identified from tensile and compression tests. A series of applications provides both at the material level and on reinforced concrete structures, for which experimental results attest to the model effectiveness.

In conclusion, this model can provide a useful tool for engineering applications, as was initially expected.

Acknowledgments

This research work was supported by the EDF utility company. The authors would like to thank EDF research and engineering departments for their valuable technical and financial input.

REFERENCES

[1] Mazars J., A description of micro and macroscale damage of concrete structure. Eng. Fract. Mech., Vol25, 1986, p729-737.

[2] Ottosen N.S., Constitutive model for short time loading of concrete. J. of Eng. Mech., ASCE, vol 105, 1979, p127-141.

[3] Mazars J., Pijaudier-Cabot G., Continuum damage theory - application to concrete, J. of Eng. Mech., ASCE, vol. 115(2), 1989, p 345–365.

[4] Jirásek M., Non-local damage mechanics with application to concrete, French Journal on Civil Engineering, vol. 8, 2004, pp. 683-707.

[5] Desmorat R., Gatuingt F., Ragueneau F., Nonlocal anisotropic damage model and related computational aspect for quasi-brittle material". Eng. Fract. Mech.. Vol 74. Num 10, 2007.

[6] Bazant Z.P., Nonlocal damage theory based on micromechanic of crack interaction, J. of Eng. Mech.. ASCE, vol. 120, pp. 593-617, 1994.

[7] La Borderie C., Mazars J., Pijaudier-Cabot G., Damage mechanics model for reinforced concrete structures under cyclic loading. A.C.I, Vol 134, 1994, p147–172, edited by W.Gerstle and Z.P. Bazant.

[8] Dragon A., Halm D., « Modélisation de l'endommagement par mésofissuration: comportement unilatéral et anisotropie induite », *C.R. Acad. Sci., Série IIb*, 1996, pp. 322 : 275-282.

[9] Pontiroli C., Rouquand A., Mazars J., Predicting concrete behaviour from quasi-static loading to hypervelocity impact. European J. of Environ. and Civil Eng., Vol. 14, N° 6-7, 2010, pp. 703-727,

[10] Desmorat R., Gatuing F., Ragueneau F., Non standard thermodynamics framework for robust computations with induced anisotropic damage., International Journal of Damage Mechanics, 2009.

[11] Drucker D.C., Prager W., Soil mechanics and plastic analysis for limit design. Quarterly of Applied Mathematics, vol. 10, no. 2, 1952, pp. 157–165.

[12] Lee J., Fenves G.L., Plastic-Damage Model for Cyclic Loading of Concrete Structures**,** J. Eng. Mech. 124, 892**,** 1998.

[13] Lemaitre J., Chaboche J.L., Mechanics of Solid Materials. Cambridge University Press, 1990.

[14] Ramtani S.**,** Contribution à la modélisation du comportement multiaxial du béton endommagé avec description du caractère unilatéral, PhD thesis, University Paris 6, 1990.

[15] Gabet T., Malecot Y., Daudeville L., Triaxial behavior of concrete under high stresses: Influence of the loading path on compaction and limit states, Cement and Concrete Research, 38(3), 403-412, 2008.

[16] Kupfer H., Hilsdorf H.K., Rüsch H.. Behavior of Concrete under Biaxial Stresses. ACI Journal, Vol. 66, No. 66-62, 1969, pp. 656-666.

[17] La Borderie C., Phénomène unilatéraux dans un matériau endommageable : Modélisation et Application à l'analyse de structures en béton. PhD thesis, Université Paris 6, 1991.

[18] Bazant Z.P., Oh B.H., Crack band theory for fracture of concrete, Materials and Structures, Vol. 16 n°3, pp. 155-177.

[19] Saouridis C., Mazars J., Prediction of the failure and size effect in concrete via a biscale damage approach, Eng Computations Journal, vol. 9, pp. 329-344, 1992.

[20] Giry C., Dufour F., Mazars J., Stress based nonlocal damage model. International J. of Solids and Structures, 48, pp.3431-3443, 2011.